JAERI-M
92-069

JT-60 UPGRADE VERTICAL STABILITY EXPERIMENTS AND ANALYSIS

May 1992

David A. HUMPHREYS* and Ryuji YOSHINO

日本原子力研究所
Japan Atomic Energy Research Institute

JAERI-M レポートは、日本原子力研究所が不定期に公刊している研究報告書です。
入手の問合わせは、日本原子力研究所技術情報部情報資料課（〒319-11茨城県那珂郡東海村）あて、お申しこしください。なお、このほかに財団法人原子力弘済会資料センター（〒319-11 茨城県那珂郡東海村日本原子力研究所内）で複写による実費頒布をおこなっております。

JAERI-M reports are issued irregularly.
Inquiries about availability of the reports should be addressed to Information Division Department of Technical Information, Japan Atomic Energy Research Institute, Tokai-mura, Naka-gun, Ibaraki-ken 319-11, Japan.

編集兼発行　日本原子力研究所
印　　刷　いばらき印刷㈱

JAERI-M 92-069

JT-60 Upgrade Vertical Stability Experiments and Analysis

David A. HUMPHREYS* and Ryuji YOSHINO

Department of Fusion Plasma Research
Naka Fusion Research Establishment
Japan Atomic Energy Research Institute
Naka-machi, Naka-gun, Ibaraki-ken

(Received April 13, 1992)

The JT-60 Upgrade tokamak, can produce plasmas with vertical elongation ($\kappa \simeq 1.6$), and thus allows investigation of vertical instability phenomena. The present work describes investigation of the vertical stability characteristics of JT-60U plasmas through experimental results and simulation. Experiments described include feedback turnoff cases and high β_p unstable plasma cases. For purposes of simulation, the plasma is modeled as a rigid assembly of current-carrying axisymmetric loops. A nominal conductor model based on design geometry was modified to reproduce the results of a series of coil excitation experiments using a reduced order system identification approach. A two-coil model was used to fit the experimental coil excitation behavior, and the full order conductor model was modified to allow the dominant modes to reflect the low order dynamic response. The resulting plasma-conductor model is shown to reproduce the vertical stability behavior of JT-60U fairly well. Theoretical predictions of limits on the value of Shafranov Λ achievable in JT-60U are made.

Keywords: Vertical Instability, High Elongation, Eddy Current, High β_p Plasma, Tokamak, Positional Control, Feedback Control, JT-60U, Simulation, Rigid Model

---

* Research Fellow

JAERI－M 92－069

JT－60U 垂直位置安定性の実験とシミュレーション計算

日本原子力研究所那珂研究所炉心プラズマ研究部
David A. HUMPHREYS* ・芳野　隆治

（1992年４月13日受理）

JT－60U トカマクは非円形度として1.6 ～1.8 のプラズマを生成するため，垂直位置不安定性現象が発生する。本論文は，JT－60U プラズマの垂直位置不安定性に関する特性を実験とシミュレーション計算の比較を行なうことにより明らかにしている。実験においては，フィードバック制御停止時の垂直位置挙動と，ベータポロイダルを高める時に発生する垂直位置不安定性を解析している。シミュレーション計算においては，プラズマをトロイダル軸対称コイルループ群のリジットな集合体と仮定し，導体に対しては，コイル励磁試験結果を再現するように，設計値を微調したモデルを使用している。すなわち，水平磁場コイルに対し仮想受動コイルを加え，真空容器渦電流モデルを低次化している。得られたプラズマー導体モデルは，プラズマ垂直位置挙動をよく再現し，これを用いて，JT－60U にて予想される，最大のシャフラノフラムダの予測計算を行なった。

那珂研究所：〒311－01　茨城県那珂郡那珂町大字向山801－１
＊リサーチ　フェロー

Contents

目　　次

1. Introduction

JT-60U, a vertically elongated, lower diverted successor to the JT-60 tokamak, began operation in March of 1991 [1]. Since that time it has produced a variety of moderately elongated ($\kappa \simeq 1.6$) plasma configurations which have provided opportunities for investigation of the passive and active vertical stability characteristics of the device. The present work describes the results of this investigation to date.

Several experiments have been performed explicitly to investigate the vertical stability characteristics of the machine. These include coil excitation tests in the absence of plasma, and feedback turnoff experiments, in which the vertical position gain is zeroed during a normal plasma discharge for intervals of several hundred milliseconds. The former experiments provided some measure of characterization of the dynamics of the actual array of toroidal current paths, allowing adjustment of a nominal conductor model to reflect the true system behavior. The latter experiments allowed testing of an overall plasma-conductor model, consisting of a rigid, current conserving plasma coupled to the modified axisymmetric conductor array.

The system identification procedure initially used a simple two-coil model to fit the horizontal field coil (H-coil) excitation behavior. For the purpose of simulating H-coil excitation tests, the conductor model including H-coil and vacuum vessel was then augmented to include a new coil. The L/R time of H-coil, the H-coil to vacuum vessel mutual inductance vector, and both the L/R time of the new coil (henceforth called "C-coil") and its inductive coupling to H-coil were adjusted to reflect the 2-coil array eigenmodes and individual circuit L/R times. For the purpose of plasma-conductor system simulations, the remainder of the nominal design PF coil model was then integrated with the modified H-coil, C-coil, and vacuum vessel to yield the new adjusted conductor model.

The rigid plasma and modified conductor model were also used to make theoretical predictions of the maximum value of Shafranov Λ achievable in JT-60U during subsequent planned high β operation.

Section 2 describes the rigid plasma, conductor array, and control models used in the analysis. The control algorithm for vertical position maintenance is discussed. Section 3 explains the system identification procedure

and salient experiments. Additional issues regarding the interpretation of coil excitation tests are discussed. Feedback turnoff and high β_p unstable plasma experimental results are presented in Section 4. Simulations of each experimental case are described and illustrated. Section 5 presents the results of stability boundary calculations addressing limits to high β_p operation. A discussion of the experimental and modeling results and conclusions are given in Section 6.

2. Rigid Plasma Vertical Stability Analysis

Simplified plasma-conductor models have often been used to analyze the vertical stability characteristics of elongated devices and design suitable control algorithms (e.g. [2–4]). Such approaches are well suited to the iterative process demanded by control design and provide a readily understandable physical picture illuminating the tradeoffs necessary in vertical stability control. The most commonly used model represents the plasma as a current-conserving, rigid body, free to move only in the vertical direction, inductively coupled to an array of discrete conductors which exert a stabilizing influence on the plasma motion [3,5].

Provided the conducting array is sufficiently close to and conformal to the plasma to provide stability on the ideal MHD time scale, the vertical instability will typically have a growth time on the order of the field penetration time of the conducting array [6]. Since this time is much longer than the Alfven time, the plasma is usually taken to be in quasiequilibrium throughout its motion. This is equivalent to setting the plasma mass to zero in the force equation. The current-conserving model has been shown to be closer to the actual energy minimizing ideal MHD eigenmode than a rigid flux-conserving plasma, providing certain generally satisfied constraints are met [7].

2.1 Plasma-Conductor Dynamic Equation

The dynamic equation describing a rigid, fixed-current plasma in quasiequilibrium, free to move only in the vertical direction, and inductively coupled

and salient experiments. Additional issues regarding the interpretation of coil excitation tests are discussed. Feedback turnoff and high β_p unstable plasma experimental results are presented in Section 4. Simulations of each experimental case are described and illustrated. Section 5 presents the results of stability boundary calculations addressing limits to high β_p operation. A discussion of the experimental and modeling results and conclusions are given in Section 6.

2. Rigid Plasma Vertical Stability Analysis

Simplified plasma-conductor models have often been used to analyze the vertical stability characteristics of elongated devices and design suitable control algorithms (e.g. [2–4]). Such approaches are well suited to the iterative process demanded by control design and provide a readily understandable physical picture illuminating the tradeoffs necessary in vertical stability control. The most commonly used model represents the plasma as a current-conserving, rigid body, free to move only in the vertical direction, inductively coupled to an array of discrete conductors which exert a stabilizing influence on the plasma motion [3,5].

Provided the conducting array is sufficiently close to and conformal to the plasma to provide stability on the ideal MHD time scale, the vertical instability will typically have a growth time on the order of the field penetration time of the conducting array [6]. Since this time is much longer than the Alfven time, the plasma is usually taken to be in quasiequilibrium throughout its motion. This is equivalent to setting the plasma mass to zero in the force equation. The current-conserving model has been shown to be closer to the actual energy minimizing ideal MHD eigenmode than a rigid flux-conserving plasma, providing certain generally satisfied constraints are met [7].

2.1 Plasma-Conductor Dynamic Equation

The dynamic equation describing a rigid, fixed-current plasma in quasiequilibrium, free to move only in the vertical direction, and inductively coupled

to a conductor array, is given by

$$\mathbf{M}\dot{\vec{I}} + \mathbf{R}\vec{I} + \left[\frac{\partial\vec{\psi}(p)}{\partial z}\frac{\partial z}{\partial\vec{I}}\right]\dot{\vec{I}} = \vec{V}. \tag{1}$$

where $\mathbf{M}$ and $\mathbf{R}$ are the conductor mutual inductance and resistance matrices, $\vec{V}$ is the applied voltage vector, and the third term represents plasma-conductor coupling and the effect of destabilizing field curvature.

Solving the force balance equation to make explicit the role of field curvature defines the third term of Eq. 1, resulting in [5]

$$\mathbf{M}\dot{\vec{I}} + \mathbf{R}\vec{I} + \frac{2R_0}{\mu_0\Gamma n}\vec{M}'_{vp}\vec{M}'_{pv}\dot{\vec{I}} = \vec{V}. \tag{2}$$

Here $\vec{M}'_{vp}$ and $\vec{M}'_{pv}$ are the mutual inductance gradient vector (from plasma to conductor array) and its transpose respectively, and $\Gamma \equiv ln|\frac{8R_0}{a}| + \Lambda - 1.5$ is the Shafranov vertical field coefficient. The decay index, n, describes the average vertical field curvature, and for a distributed plasma current is properly given by

$$n \equiv -\frac{1}{I_p B_{z0}}\int RJ_\phi\left(\frac{\partial B_R}{\partial z}\right)\mathrm{d}R\mathrm{d}z, \tag{3}$$

where the integral is performed over the plasma poloidal cross section.

Solutions of Eq. 1 or Eq. 2 typically consist of a set of conductor current eigenmodes and corresponding eigenvalues, one of which is unstable. The remainder of the modes correspond essentially to decay modes of the conductor array with very little coupling to plasma motion.

2.2 JT-60U Model

The nominal conductor array used in the JT-60U analysis is illustrated in Fig. 1. This array was calculated based on the design geometry for the device, and includes all poloidal field (PF) coil and vacuum vessel toroidal conducting paths [8]. The vacuum vessel is represented by a discretized array of 100 elements, each of whose resistances and self inductances were chosen to match the local values of the corresponding path. Mutual inductances were calculated using the coupled filament approximation.

The dominant up-down antisymmetric current mode of the nominal vacuum vessel model has a decay time constant of about 8 msec, while the nominal H-coil L/R time is about 280 msec.

The plasma current distribution is represented as either a single filament located at the current centroid, or a multifilament uniform current density array matching the elongation and position of the plasma, The single filament and uniform current distribution models represent two reasonable extremes in plasma-conductor coupling efficiency, and thus allow bracketing of plasma response over the range of physically realizable current distributions.

2.3 Control Algorithm

Vertical stability control is provided by driving H-coil alone with a feedback relation which determines voltage demand as a function of estimated plasma vertical position. Proportional and derivative (velocity) feedback is provided. The overall feedback loop calculation and power supply delay has been estimated to be nominally about 2 msec. In addition, H-coil current feedback is applied, artificially reducing the effective resistance of H-coil to a negative value [8].

Using a single-pole model of the power supply delay [9], the feedback transfer function describing voltage applied to H-coil is given by

$$V_H(s) = R_H^{prog} I_H(s) - \frac{G_p(1+\tau_d s)}{(1+\tau_{ps} s)} z_{pred}(s) \qquad (4)$$

where the predicted vertical position, z_{pred}, is a function of magnetic signals, and can therefore be expressed as a function of conductor currents, $\vec{I}$. G_p is the proportional gain, τ_d is the derivative gain time constant, and τ_{ps} is the power supply delay time, taken to be 2 msec. R_H^{prog} represents the programmed H-coil resistance reduction factor.

3. System Identification

The response of the nominal conductor model including only H-coil and vacuum vessel to a forced current ramp in H-coil is shown in Fig. 2 along with experimental data from such a test. The case shown corresponds to a current

The dominant up-down antisymmetric current mode of the nominal vacuum vessel model has a decay time constant of about 8 msec, while the nominal H-coil L/R time is about 280 msec.

The plasma current distribution is represented as either a single filament located at the current centroid, or a multifilament uniform current density array matching the elongation and position of the plasma, The single filament and uniform current distribution models represent two reasonable extremes in plasma-conductor coupling efficiency, and thus allow bracketing of plasma response over the range of physically realizable current distributions.

2.3 Control Algorithm

Vertical stability control is provided by driving H-coil alone with a feedback relation which determines voltage demand as a function of estimated plasma vertical position. Proportional and derivative (velocity) feedback is provided. The overall feedback loop calculation and power supply delay has been estimated to be nominally about 2 msec. In addition, H-coil current feedback is applied, artificially reducing the effective resistance of H-coil to a negative value [8].

Using a single-pole model of the power supply delay [9], the feedback transfer function describing voltage applied to H-coil is given by

$$V_H(s) = R_H^{prog} I_H(s) - \frac{G_p(1+\tau_d s)}{(1+\tau_{ps} s)} z_{pred}(s) \qquad (4)$$

where the predicted vertical position, z_{pred}, is a function of magnetic signals, and can therefore be expressed as a function of conductor currents, $\vec{I}$. G_p is the proportional gain, τ_d is the derivative gain time constant, and τ_{ps} is the power supply delay time, taken to be 2 msec. R_H^{prog} represents the programmed H-coil resistance reduction factor.

3. System Identification

The response of the nominal conductor model including only H-coil and vacuum vessel to a forced current ramp in H-coil is shown in Fig. 2 along with experimental data from such a test. The case shown corresponds to a current

ramp rate of $\dot{I}_H = 10.8\ kA/sec$. The figure shows the voltage required to drive the programmed current, and thus reflects the response of H-coil and its coupling with vacuum vessel modes. The nominal conductor model behaves significantly differently from the actual coil excitation response, indicating some combination of inaccuracy and missing current paths in the conductor model.

Similarly, the actual measured frequency response of H-coil is shown in Fig. 3 as a frequency-varying impedance: $Z(f) = R(f) + j2\pi f L(f)$ (where f is frequency in Hz). The variation of impedance with frequency reflects the presence of conducting paths (such as the vacuum vessel) coupled to H-coil and possibly such frequency-dependent phenomena as the conductor skin effect. The figure also shows the result of a simulated H-coil excitation using the nominal conductor array model. This comparison also reveals a discrepancy between model and experimental result.

In the absence of more accurate measurements and experimental data to determine the location of possible missing current paths, a reduced order system identification analysis was performed in order to adjust the nominal conductor model to approximately reproduce the observed system response.

Because the only PF coil which both strongly affects vertical stability and can be directly excited by power supplies is the H-coil, only H-coil circuit quantities and H-coil to vacuum vessel coupling were addressed by in the system identification effort.

Both current ramp (time domain) and frequency response data were used to characterize the actual system response. The current ramp response is dominantly second order, all higher order behavior being unresolvable due to the intrinsic noise level. Although good estimates of the uncertainties governing the frequency response data are not available, low frequency divergence of measurements from the known DC values suggests that in this case as well, more than two poles cannot be accurately resolved. Despite that indication of measurement error, the high frequency behavior suggests the presence of higher order modes, making the overall frequency data difficult to fit with only two poles. At best, therefore, the frequency data can only be used for rough benchmarking of the reduced order model. With these limitations, the reduced order system used for fitting is therefore second order, representing the H-coil and some appropriate composite vacuum vessel and

unknown conductor mode. Both ramp and frequency response experiments were performed with all PF circuits except H-coil open circuited.

The circuit equation describing H-coil coupling with a composite secondary circuit (for which we shall use the subscript "c") is

$$\mathbf{M}_2\dot{I} + \mathbf{R}_2 I = \begin{bmatrix} 1 \\ 0 \end{bmatrix} V_H, \tag{5}$$

where $\mathbf{M}_2$ and $\mathbf{R}_2$ are the 2×2 inductance and resistance matrices, $\vec{I}$ is the current vector, and V_H is the voltage applied to H-coil.

We first address the current ramp response analysis.

3.1 Current Ramp Response Analysis

We consider the solution of Eq. 5 for a forced current ramp applied to H-coil:

$$I_H = \dot{I}_{H0} t \quad t \geq 0. \tag{6}$$

The voltage required to produce the current ramp can be easily shown to be

$$V_H(t) = L_H \dot{I}_{H0} + R_H \dot{I}_{H0} t - \frac{M_{Hc}^2}{L_c} \dot{I}_{H0} e^{-\frac{R_c}{L_c} t}. \tag{7}$$

Note that only four system quantities can be determined from the four free parameters in the solution. Since there are 5 unknowns in the two-coil system, either R_c or L_c must be defined ad hoc or determined from some other source to close the system.

Fixing the long-term (linear ramp) voltage behavior, the error between a function of this form and the experimental data from two ramp response experiments such as that shown in Fig. 2 is minimized in the least squares sense by the choices shown in Table 1.

These circuit values yield the fit shown in Fig. 4 and allow characterization of the self inductance and resistance of H-coil. Notice that these values identify the eigenvalues of the reduced system as 337 msec (predominantly H-coil current) and 2.56 msec (predominantly C-circuit current).

Table 1 Two coil circuit values to fit ramp response.

Quantity	Value	units
L_H	1550.	μH
R_H	4900.	$\mu\Omega$
$\frac{M_{Hc}^2}{L_c}$	1370.	μH
$\frac{L_c}{R_c}$	23.6	msec

3.2 *Frequency Response Analysis*

Data from frequency excitation of H-coil (shown in Fig. 3) poses some problems for interpretation. It does not appear to exhibit the shape characteristic of two coupled circuits. For example, Fig. 5 shows the frequency response of the nominal H-coil + vacuum vessel model system, displaying the saturation at both low and high frequencies which is characteristic of two coupled circuits. In fact it is easily shown that for the two coil system described by Eq. 5, the frequency dependent resistance and inductance are given by

$$R(\omega) = R_H \left\{ \frac{1 + (\tau_{22}^2 + \tau_{12}\tau_{21})\omega^2}{1 + \tau_{22}^2\omega^2} \right\} \tag{8}$$

and

$$L(\omega) = L_H \left\{ \frac{1 + (\tau_{22}^2 - \frac{\tau_{22}}{\tau_{11}}\tau_{12}\tau_{21})\omega^2}{1 + \tau_{22}^2\omega^2} \right\}, \tag{9}$$

where $\tau_{11} = L_H/R_H$, $\tau_{12} = M_{Hc}/R_H$, $\tau_{21} = M_{Hc}/R_c$, and $\tau_{22} = L_c/R_c$. The two response curves share the same pole, but have different zeros. Examination of the ordering resulting from the two-coil model data of Table 1 reveals that the $R(\omega)$ zero frequency, Z_R, the pole, $1/\tau_{22}$, and the $L(\omega)$ zero frequency, Z_L, are ordered such that

$$Z_R < \frac{1}{\tau_{22}} < Z_L, \tag{10}$$

consistent with the slopes of the experimental curves. Nevertheless, although the experimental data lacks reliable error bars, the model response appears here, as in the nominal ramp response case, to be significantly different from the experimental result. The difference in this case does not appear to be

merely due to inaccuracies in the conductor model, as the dominant zeros would have to be moved very far to account for the data. Either the data is not reliable, or there are other current paths carrying large currents, or another frequency effect exists which is not being accounted for in the simple model.

In this latter regard, it is important to consider one other contribution to the frequency dependent impedance: that of skin depth effects.

3.2.1 Skin Depth Effects in Frequency Response

The small toroidal windings making up a large PF magnet in a high aspect ratio tokamak tend to be thin enough that for typical frequencies of interest in axisymmetric control, the finite skin depth does not significantly affect their impedance. For example, for a frequency of 100 Hz (higher than typical vertical instability growth rates in present tokamaks), the skin depth of room temperature copper is 6.6 mm. By comparison, individual windings in the JET tokamak have a typical radius of 2-5 mm [10], so that PF coil skin depth effects are indeed not important in JET.

However, JT-60U possesses windings which are significantly larger. H-coil is made up of rectangular windings with typical narrowest widths of 4-5 cm in order to withstand a large stress caused by high current disruptions. A skin depth of 2 cm corresponds to a frequency of about 10 Hz. For frequencies much above this value, the frequency dependence of PF coil impedances must be taken into account. For the range of experiments performed to date in JT-60U, the vertical instability growth rates in the presence of active feedback have not exceeded 3 rad/sec (corresponding to 19 Hz), although passive growth rates have been calculated to be as high as 180 rad/sec (corresponding to 29 Hz). Skin depth effects should not therefore be significant for experimental results to date.

The frequency response testing of H-coil did, however, significantly exceed this rough limit. Therefore to properly understand the physics involved in those results we must examine the effect of finite skin depth.

To accurately model the complicated geometry of H-coil, composed of 26 turns of varying rectangular cross section, is beyond the scope of this work. Instead we choose a simpler conductor model in which the current

density solution is well known [11]. We consider a long, straight, circular cross section conductor in an oscillatory axial electric field whose magnitude is uniform and fixed at the surface of the conductor. This would describe a circular cross section high aspect ratio PF coil winding under the influence of the E-field imposed by a ramping ohmic heating coil, for example. The current profile in such a conductor is easily derived, and consists of a sum of Kelvin functions. For an applied surface E-field given by

$$\vec{E}(t) = E_0 e^{i\omega t}\hat{z} \tag{11}$$

where $\hat{z}$ represents the axial direction, the current profile solution is

$$\vec{J}(r,t) = J_0 \left\{\mathrm{ber}(kr) + i\,\mathrm{bei}(kr)\right\} e^{i\omega t}\hat{z} \tag{12}$$

where $k^2 \equiv \frac{\mu_0\omega}{\eta}$, η is the resistivity of the conductor, and J_0 is the (complex) central current density, determined by the surface E-field boundary condition.

The corresponding effective impedance found by integrating the current density over the conductor cross section is

$$\mathcal{Z} = \mathcal{R} + i\omega\mathcal{L} = \frac{ka\mathcal{R}_0}{2}\left\{\frac{\mathrm{ber}(ka) + i\,\mathrm{bei}(ka)}{\mathrm{bei}'(ka) - i\,\mathrm{ber}'(ka)}\right\}, \tag{13}$$

where $\mathcal{R}_0$ is the DC resistance of the conductor and the prime ($'$) denotes the derivative of the Kelvin functions with respect to the argument.

This solution exhibits the familiar edge-localized current density phenomenon known as the skin effect. Of course, the skin effect contribution to the self inductance in general only affects the internal inductance of the coil, and is thus a small perturbation on the total self inductance of a typical axisymmetric toroidal coil. However, the contribution to the resistance can be significant.

Modeling H-coil as such a long conductor with an effective radius of 2 cm, we find the variation in resistance and internal inductance of H-coil shown in Fig. 6. Using a nominal H-coil resistance of 4.9 mΩ, we find that at 100 Hz the effective resistance of H-coil due to skin effects alone is 8.7 mΩ, while the effective resistance due to vessel coupling alone is 177 mΩ. The skin depth augmentation of only a few percent is thus quite negligible.

It should be noted, however, that if conducting structures and magnets become larger as tokamaks grow to satisfy the requirements of power reactors,

the importance of skin effects for comparable frequencies may also become greater. This observation is, of course, somewhat offset by the simultaneous reduction of characteristic instability growth rates in larger devices. The relative influence of these two competing phenomena will have to be investigated in more detail for each new design.

3.3 Mapping Reduced Order to Full Order

Having determined the two-circuit reduced order parameters to satisfactorily fit the observed ramp and (low) frequency response data, it is necessary to map the reduced order system response to the full order model. We wish to modify the full order system (consisting of H-coil and the 100 element vacuum vessel model) to make use of the new data available, while still preserving the dynamic response of the higher order modes.

If the vacuum vessel and H-coil models accounted sufficiently well for the toroidal current paths in the system, modification of these circuits alone would serve to reproduce both coil excitation data and plasma response. However, the characteristic time of the two-coil model C-circuit was found to be 23.6 msec (see Table 1). For the dominant vacuum vessel up-down antisymmetric mode to respond with this time constant would require an effective uniform increase of the conductivity by a factor of 3. This is too great an error to reasonably expect to be explained by disparity between design and construction. Moreover, the degree of stability conferred upon the plasma by such a change in the eigenvalue corresponding to the dominant midplane-antisymmetric vessel mode stabilizes the vertical instability far beyond experimentally observed thresholds. This large disparity strongly suggests the presence of toroidal current paths in the actual device which are not accounted for in the nominal conductor model.

In order to properly account for the coil excitation and plasma response observations, we must therefore augment the system with an additional circuit and choose the inductive coupling and L/R time to fit the excitation data. For such an approach to be consistent and successful, the additional current paths must couple to the plasma and vessel in a way similar to that of H-coil. If this is true, the extra coil can introduce sufficient additional dynamics to H-coil to reproduce the actual aggregate reponse.

Following this procedure, we fix L_H and R_H to the values given in Table 1 and add an extra coil to the H-coil plus vacuum vessel system, so that the augmented mutual inductance matrix appears as

$$\mathrm{M}_{aug} = \begin{bmatrix} L_H & M_{CH} & f_{VH}\vec{M}_{VH}^T \\ M_{CH} & L_C & f_{VC}\vec{M}_{VC}^T \\ f_{VH}\vec{M}_{VH} & f_{VC}\vec{M}_{VC} & \mathrm{M}_{VV} \end{bmatrix} \tag{14}$$

where each entry is the submatrix indicated by the subscripts: boldface indicates a square matrix, and regular typeface indicates a scalar except where explicitly labeled as a vector. f_{VH} and f_{VC} are scale factors. Similarly, the resistance matrix is given by

$$\mathrm{R}_{aug} = \begin{bmatrix} R_H & 0 & \vec{0}^T \\ 0 & R_C & \vec{0}^T \\ \vec{0} & \vec{0} & \mathrm{R}_{VV} \end{bmatrix} \tag{15}$$

where $\mathbf{R}_{VV}$ is the diagonal vessel resistance matrix.

The scale factors f_{VH} and f_{VC}, as well as the form of $\vec{M}_{VC}$ can then be adjusted so that the initial H-coil voltage at the onset of current ramp is matched by the modified system response and to improve frequency response. Either L_C or R_C must be chosen ad hoc to close the system.

The ramp and frequency responses of the matrices resulting from this procedure are shown in Figs. 7 and 8. The ramp response is indistinguishable from the two-coil model ramp response of Fig. 4. The frequency response shows a relatively good fit to the effective resistance over the frequency range below 20 Hz, but the effective inductance is not so well matched. Nevertheless, there is a fairly good match over the narrow but important range of $1Hz < f < 10Hz$, into which typical growth rates for the JT-60U cases simulated fall. In addition, as mentioned before, the low frequency behavior of the experimental frequency response data is not physical.

Note that the characteristic L/R time of the hypothetical missing current path modeled by the C-coil augmentation is long compared to the dominant up-down antisymmetric vacuum vessel mode response time. This suggests that the missing circuit may be either a low conductivity path of large poloidal cross-section or a copper pathway of smaller cross-section.

The modified model resulting from the low order fit and full order augmentation system identification procedure was then used in simulating JT-60U vertical stability experiments. In the next section we describe experimental results from selected examples of two types of discharges and simulations thereof using the modified conductor model.

4. Experimental Results and Simulation

We describe two types of experiments which provide data on the vertical stability of JT-60U equilibria and allow assessment of the accuracy of the simulation models: those for which vertical position feedback gain was set to zero over a fixed interval during a shot, and those in which β_p rose over the course of a shot due to applied NBI heating, resulting in onset of vertical instability. Simulations of several examples of these shots were calculated using the conductor array model adjusted to reflect the system identification parameters described in Sec. 3.

4.1 Feedback Turnoff Experiments

A series of experiments were performed in which the proportional gain, G_p, (see Eq. 4), was set to zero, removing all vertical position feedback for intervals of 300 msec or 600 msec. However, the value of R_H^{prog} was held fixed over the turnoff interval. During typical 300 msec turnoff periods the plasma moved monotonically away from the original equilibrium vertical position until control was restored. 600 msec turnoff periods typically exhibited establishment of a new stable equilibrium before proportional control gain was restored.

Examples of this motion are shown in Figs. 9 and 10, illustrating a typical 300 msec and 600 msec gain turnoff interval respectively. These figures show vertical position measured by magnetic signals, and compare the experimental data to simulations of the turnoff intervals using the rigid plasma model. The simulation reproduces the experimental motion within an uncertainty of a few millimeters, comparable to the accuracy of the position measurement itself.

Nevertheless, possible indications of missing conductor dynamics can be

The modified model resulting from the low order fit and full order augmentation system identification procedure was then used in simulating JT-60U vertical stability experiments. In the next section we describe experimental results from selected examples of two types of discharges and simulations thereof using the modified conductor model.

4. Experimental Results and Simulation

We describe two types of experiments which provide data on the vertical stability of JT-60U equilibria and allow assessment of the accuracy of the simulation models: those for which vertical position feedback gain was set to zero over a fixed interval during a shot, and those in which β_p rose over the course of a shot due to applied NBI heating, resulting in onset of vertical instability. Simulations of several examples of these shots were calculated using the conductor array model adjusted to reflect the system identification parameters described in Sec. 3.

4.1 Feedback Turnoff Experiments

A series of experiments were performed in which the proportional gain, G_p, (see Eq. 4), was set to zero, removing all vertical position feedback for intervals of 300 msec or 600 msec. However, the value of R_H^{prog} was held fixed over the turnoff interval. During typical 300 msec turnoff periods the plasma moved monotonically away from the original equilibrium vertical position until control was restored. 600 msec turnoff periods typically exhibited establishment of a new stable equilibrium before proportional control gain was restored.

Examples of this motion are shown in Figs. 9 and 10, illustrating a typical 300 msec and 600 msec gain turnoff interval respectively. These figures show vertical position measured by magnetic signals, and compare the experimental data to simulations of the turnoff intervals using the rigid plasma model. The simulation reproduces the experimental motion within an uncertainty of a few millimeters, comparable to the accuracy of the position measurement itself.

Nevertheless, possible indications of missing conductor dynamics can be

seen in the differing degrees of overshoot between experimental and simulation results in Fig. 10b and the similarly differing apparent time constants in Fig. 9b.

In JT-60U the presence of $R_H^{prog} > R_H(actual)$ results in an effectively negative H-coil resistance, exerting a stabilizing influence on the plasma. The absence of an integral term ($\propto \int z\mathrm{d}t$) in the feedback law results in a steady-state non-zero offset in vertical position from the reference signal. The feedback system therefore applies a non-zero steady-state voltage to H-coil, contributing to the equilibrium. The zeroing of G_p applies an effective voltage step to H-coil, driving the plasma to a new equilibrium. This process is stable for sufficiently low decay index due to the stabilizing effect of R_H^{prog}, as can be seen in the longer interval case of Fig. 10.

4.2 *High β_p Unstable Plasmas*

During the course of several neutral beam-heated shots, β_p became sufficiently high that the preset control gains could not stabilize the plasma. These cases provided an opportunity to compare simulation predictions with actual unstable plasma behavior. Results of two shots with particularly clear underdamped vertical instability growth are shown in Figs. 11 and 12. Fig. 11 shows vertical position, simulation-predicted growth rates, and β_p evolution as a function of time. The actual maximum growth rate was found to be $\gamma_{exp} \simeq 8 \pm 130i$, and the predicted value was calculated to be $\gamma_{sim} \simeq 7 \pm 290i$. The plasma was lost at the end of the time interval shown. Experimental onset of instability and real growth rate coincide well with the predicted values. The discrepancy in the imaginary part is in part attributable to the single pole power supply model and the overall neglect of the discrete nature of the control system.

Fig. 12 shows vertical position and β_p as a function of time for a case in which β_p decreased before the plasma was lost, allowing control to be reestablished. The figure shows the onset of instability and restoration of control coinciding with the same approximate value of β_p. The actual maximum growth rate was found to be $\gamma_{exp} \simeq 15 \pm 190i$, and the predicted value was calculated to be $\gamma_{sim} \simeq 14 \pm 530i$. Again, the experimental real growth rate coincides well with the predicted value.

5. Stability Boundary Calculations

Analysis of expected vertical stability limits for JT-60U was carried out using the simple rigid plasma model and adjusted conductor array described in Secs. 2 and 3. Both a single filament and uniform current distribution multifilament plasma model are used along with the full conductor array to calculate critical decay indices for ideal MHD stability limits. The gain space is then searched to determine the maximum stabilizable value of the Shafranov $\Lambda \equiv \beta_p + l_i/2$.

5.1 Critical Decay Index

The critical decay index, n_c, describes the field curvature beyond which a plasma becomes vertically unstable on the ideal MHD timescale [9], corresponding to infinite growth rate for a massless plasma. Allowing $\gamma \rightarrow \infty$ as $n \rightarrow n_c$ in Eq. 2, it can be easily shown that for an array of stabilizing conducting elements, n_c is given by

$$n_c = -\frac{2R_0}{\mu_0 \Gamma} Tr(\mathrm{M}^{-1} \vec{M}'_{vp} \vec{M}'_{pv}), \tag{16}$$

where Tr indicates the matrix trace.

Fig. 13 shows critical decay index magnitude for both single filament (SF) and multifilament (MF) plasma models plotted as a function of Λ. Also shown (triangles) are experimental decay index magnitudes and Λ values achieved in JT-60U to date for $\kappa \simeq 1.6$ equilibria. The maximum n/n_c achieved corresponds to $n \sim 88\%$ of the multifilament critical index or 80% of the single filament critical index, at $\Lambda \simeq 2.7$. Extrapolating this data for $n = -1.6$, corresponding to elongation $\kappa \simeq 1.6$, $\Lambda \sim 3.5$ appears to be the theoretical upper limit achievable in JT-60U (corresponding to the single filament, or most favorable, model). Passive growth rate and active control calculations necessary to determine a more realistic limit are examined in the next section.

5.2 *Passive and Active Calculations*

Single filament passive and active responses for fixed decay index are now examined to determine a more realistic upper limit to achievable Λ. Fig. 14 shows calculated single filament model passive growth rates for $n = -1.6$ as a function of Λ. Since the nominal feedback loop plus power supply delay time is about 2 msec, the $\gamma \simeq 500$ sec^{-1} crossover point provides an approximate measure of the controllability limit [9], and predicts $\Lambda_{max} \simeq 3.0$.

Figs. 15 and 16 show active stability boundaries calculated in $G_p - \tau_d$ space using the single pole, PD power supply model described in Section 2.1.8. Fig. 15, corresponding to $\Lambda = 3.0$, reveals a broad stable region, while Fig. 16 shows that $\Lambda = 3.1$ cannot be stabilized for any combination of values of G_p and τ_d.

6. Discussion and Conclusions

A series of experiments have been conducted on the JT-60 Upgrade device which allowed assessment of the vertical stability characteristics of the machine. Simulations of feedback disabled intervals and discharges which became fortuitously unstable were simulated using a rigid plasma model and both a nominal, design-based conductor model and a system identification-based improved conductor model. In addition, a set of coil excitation tests were performed which measured H-coil and vacuum vessel circuit characteristics.

Simulation of coil excitation tests revealed significant inaccuracy in the nominal conductor model. This observation motivated the the use of excitation data to modify the nominal conductor model. The degree of disparity between the initial simulation and experimental results suggests that current paths exist in the device which are missing from the nominal conductor model.

A reduced order system identification procedure was followed and the nominal full order model was modified and augmented to reproduce the (H-coil and vessel) conductor response. Addition of an artificial circuit yielded a modified conductor model which proved capable of reproducing both coil excitation and vertical instability data fairly well, especially in the frequency

5.2 *Passive and Active Calculations*

Single filament passive and active responses for fixed decay index are now examined to determine a more realistic upper limit to achievable Λ. Fig. 14 shows calculated single filament model passive growth rates for $n = -1.6$ as a function of Λ. Since the nominal feedback loop plus power supply delay time is about 2 msec, the $\gamma \simeq 500$ sec^{-1} crossover point provides an approximate measure of the controllability limit [9], and predicts $\Lambda_{max} \simeq 3.0$.

Figs. 15 and 16 show active stability boundaries calculated in $G_p - \tau_d$ space using the single pole, PD power supply model described in Section 2.1.8. Fig. 15, corresponding to $\Lambda = 3.0$, reveals a broad stable region, while Fig. 16 shows that $\Lambda = 3.1$ cannot be stabilized for any combination of values of G_p and τ_d.

6. Discussion and Conclusions

A series of experiments have been conducted on the JT-60 Upgrade device which allowed assessment of the vertical stability characteristics of the machine. Simulations of feedback disabled intervals and discharges which became fortuitously unstable were simulated using a rigid plasma model and both a nominal, design-based conductor model and a system identification-based improved conductor model. In addition, a set of coil excitation tests were performed which measured H-coil and vacuum vessel circuit characteristics.

Simulation of coil excitation tests revealed significant inaccuracy in the nominal conductor model. This observation motivated the the use of excitation data to modify the nominal conductor model. The degree of disparity between the initial simulation and experimental results suggests that current paths exist in the device which are missing from the nominal conductor model.

A reduced order system identification procedure was followed and the nominal full order model was modified and augmented to reproduce the (H-coil and vessel) conductor response. Addition of an artificial circuit yielded a modified conductor model which proved capable of reproducing both coil excitation and vertical instability data fairly well, especially in the frequency

range of instability growth rates observed in JT-60U discharges to date.

The issue of frequency dependent conductor resistance variation due to skin depth effects was addressed. Although calculation showed that the effect is not great in JT-60U, the use of large conductors in later devices may necessitate the inclusion of finite penetration depth effects in stability calculations.

The maximum achievable value of Shafranov Λ was studied using the augmented conductor and rigid plasma models. Analysis indicates that an upper limit is given approximately by $\Lambda_{max} \simeq 3.0$, since $\Lambda = 3.1$ is found to be unstabilizable for any gain values. This prediction is likely to be somewhat optimistic, since rigid, current-conserving vertical motion does not constitute the actual energy-minimizing eigenmode. The impact of this limit on maximum achievable β_p has not been assessed, and will require more detailed analysis of current profile (l_i) effects.

Acknowledgements

Authors would like to thank the reseachers of the Large Tokamak Experiment Division I and the JT-60U Facility Division I. One of the authors (D.A.Humphreys) wants to express his gratitude to Drs. T.Kimura, K.Kurihara, and H.Ninomiya for their continuous support and encouragement.

range of instability growth rates observed in JT-60U discharges to date.

The issue of frequency dependent conductor resistance variation due to skin depth effects was addressed. Although calculation showed that the effect is not great in JT-60U, the use of large conductors in later devices may necessitate the inclusion of finite penetration depth effects in stability calculations.

The maximum achievable value of Shafranov Λ was studied using the augmented conductor and rigid plasma models. Analysis indicates that an upper limit is given approximately by $\Lambda_{max} \simeq 3.0$, since $\Lambda = 3.1$ is found to be unstabilizable for any gain values. This prediction is likely to be somewhat optimistic, since rigid, current-conserving vertical motion does not constitute the actual energy-minimizing eigenmode. The impact of this limit on maximum achievable β_p has not been assessed, and will require more detailed analysis of current profile (l_i) effects.

Acknowledgements

Authors would like to thank the reseachers of the Large Tokamak Experiment Division I and the JT-60U Facility Division I. One of the authors (D.A.Humphreys) wants to express his gratitude to Drs. T.Kimura, K.Kurihara, and H.Ninomiya for their continuous support and encouragement.

References

[1] NINOMIYA, H., ANDO, T., et al, Plasma Devices and Operations **1** (1990) 43

[2] FUKUYAMA, A., SEKI, S., et al, Jpn. J. of Appl. Phys. **14** (1975) 871

[3] JARDIN, S. and LARRABEE, D., Nucl. Fusion **22** (1982) 1095

[4] NEILSON, G., DYER., G. R., et al, Nucl. Fus. **24** (1984) 1291

[5] LAZARUS, E.A., LISTER, J.B., NEILSON, G.H., Nucl. Fusion **30** (1990) 111

[6] WESSON, J. A., Nucl. Fus. **18** (1978) 87

[7] HUTCHINSON, I. H., Nucl. Fus. **29** (1989) 2107

[8] YOSHINO, R., JAERI-Memo 03-088, Japan Atomic Energy Res. Inst., March 1991

[9] HUMPHREYS, D. A., HUTCHINSON, I. H., Filament-Circuit Model Analysis of Alcator C-MOD Vertical Stability, PFC Rept. PFC/JA-89-28, Mass. Inst. of Tech., Cambridge, (1989)

[10] BONICELLI, T., private communication

[11] RELTON, F. E., Applied Bessel Functions, Blackie, London, 1946, pp. 176ff

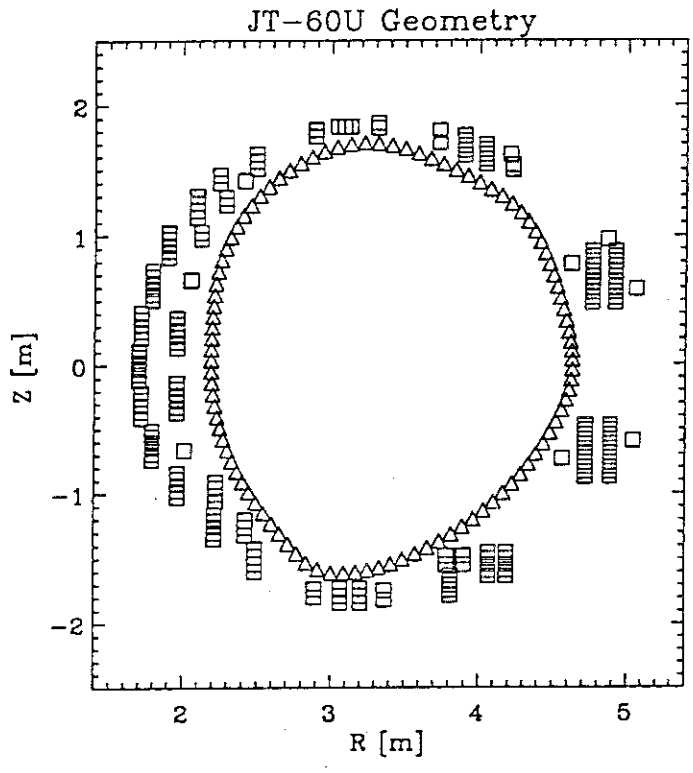

Fig. 1 Geometry of JT-60U conductor model.

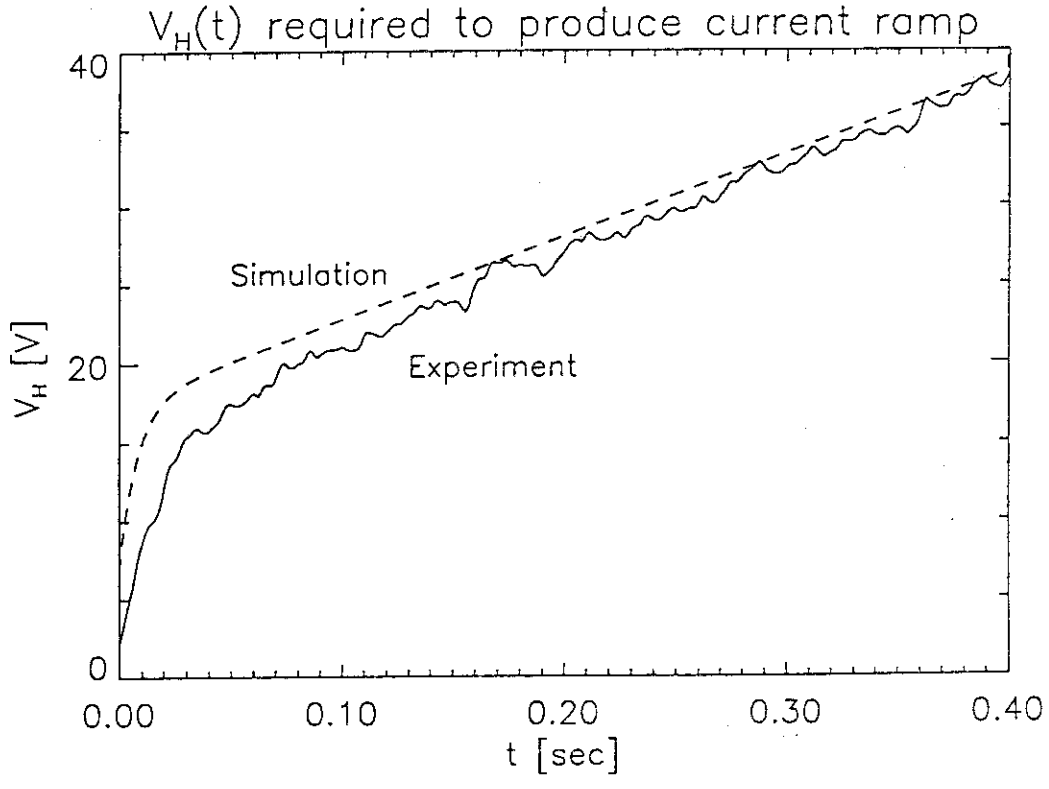

Fig. 2 Experimentally measured and nominal conductor model simulation of voltage required to drive current ramp demand in H-coil.

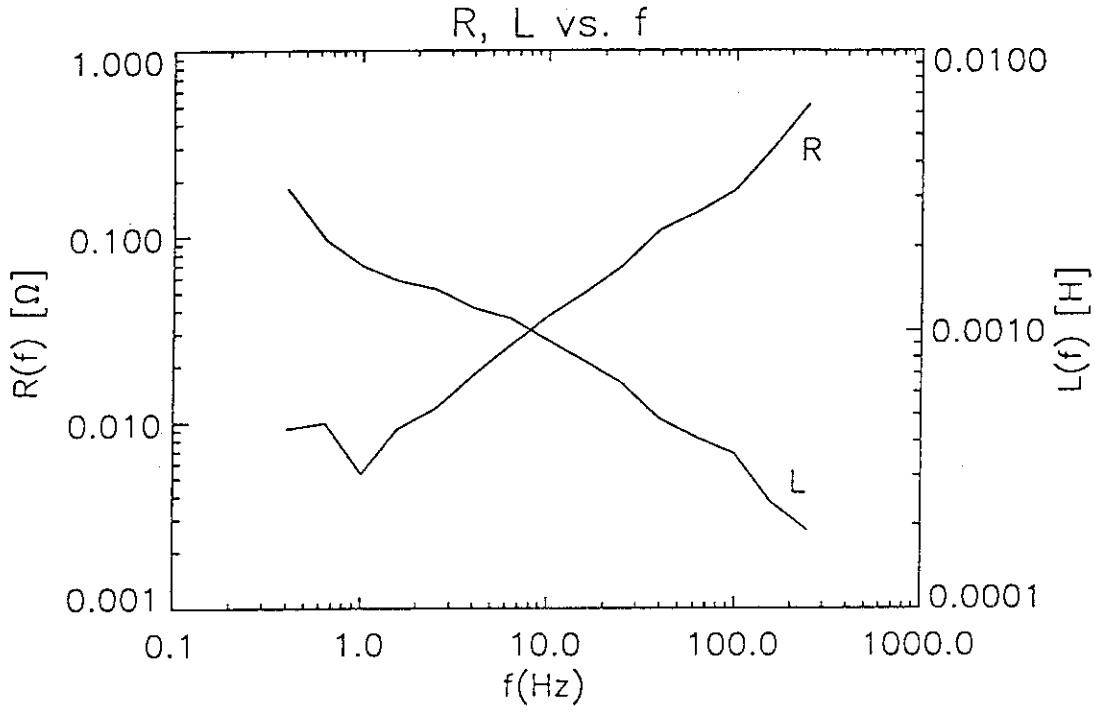

Fig. 3 Experimentally measured frequency response of H-coil.

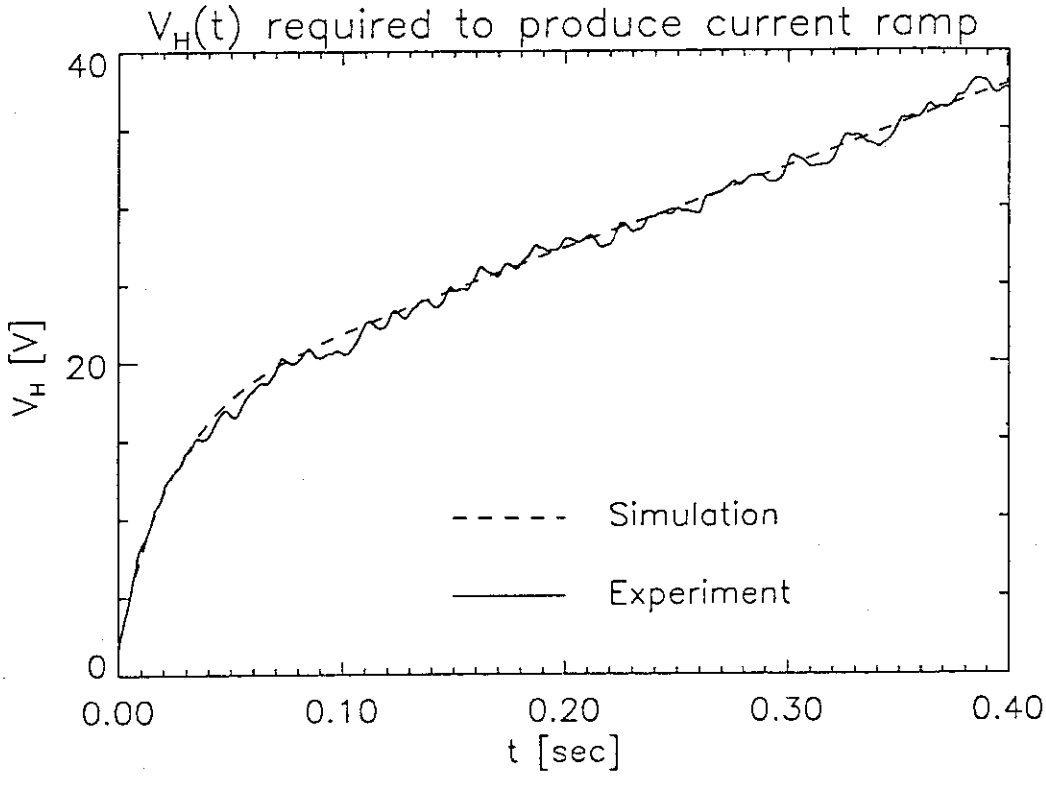

Fig. 4 Experimentally measured and 2-coil model fit of voltage required to drive current ramp demand in H-coil.

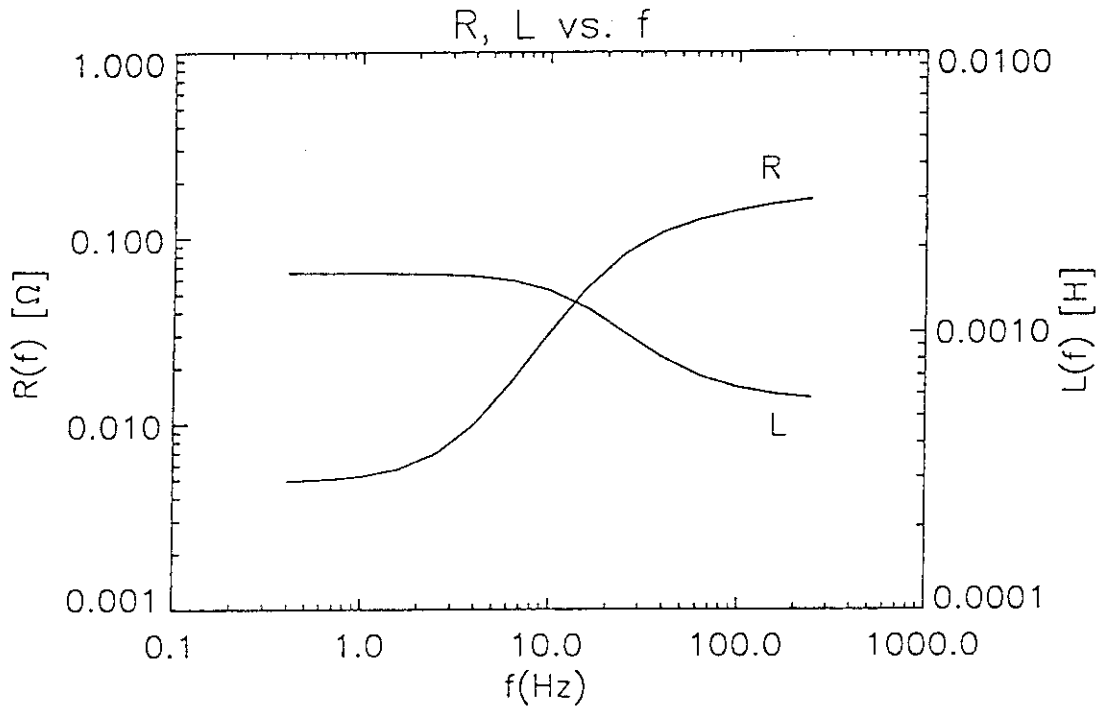

Fig. 5 Frequency response of H-coil simulated with nominal conductor model.

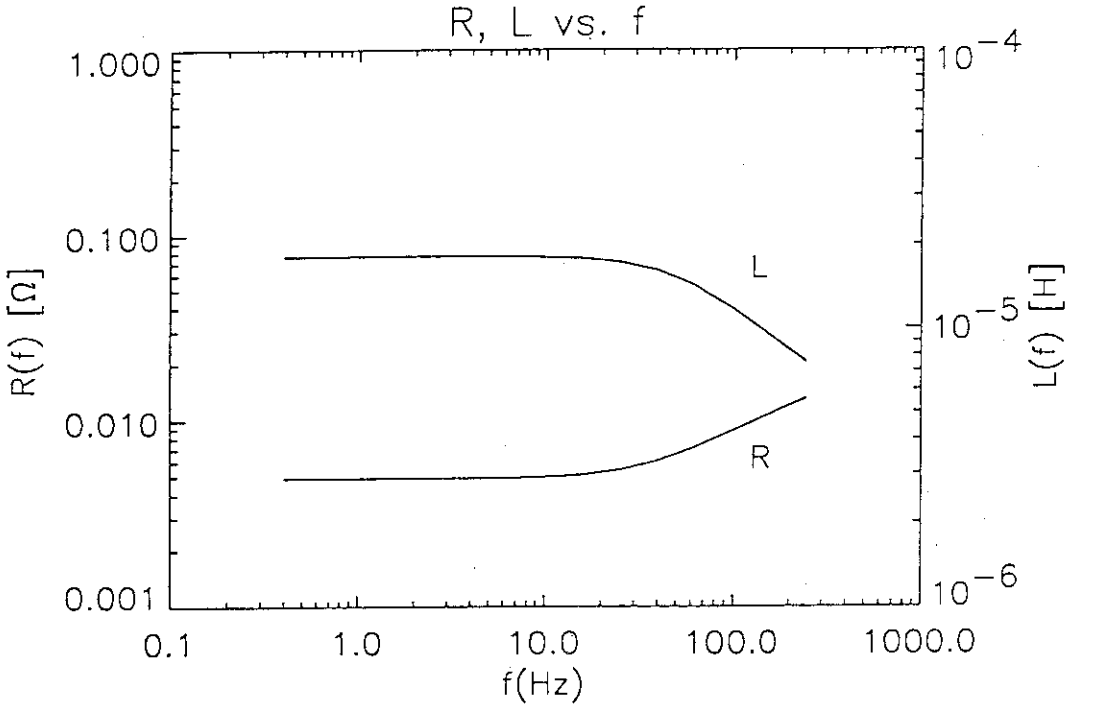

Fig. 6 Frequency dependent variation in effective resistance, R, and internal inductance, L, of long cylindrical conductor with 2 cm radius and DC resistance equal to the system-identified DC resistance of H-coil.

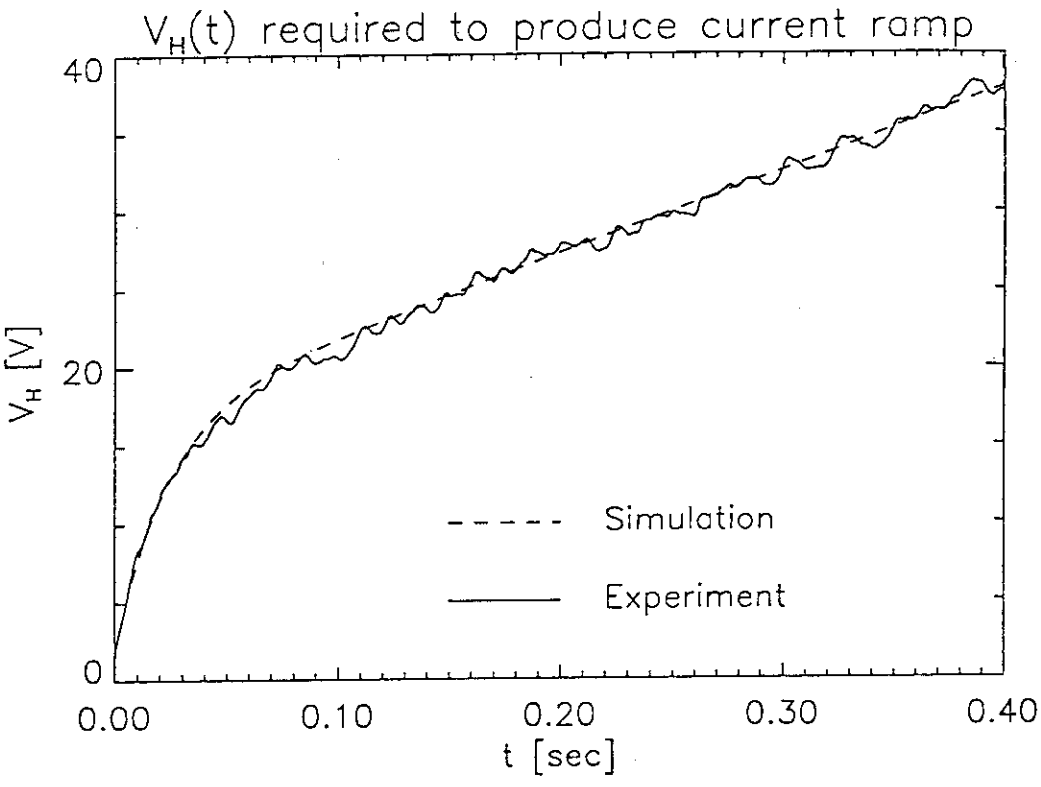

Fig. 7 Experimentally measured and modified conductor model fit of voltage required to drive current ramp demand in H-coil.

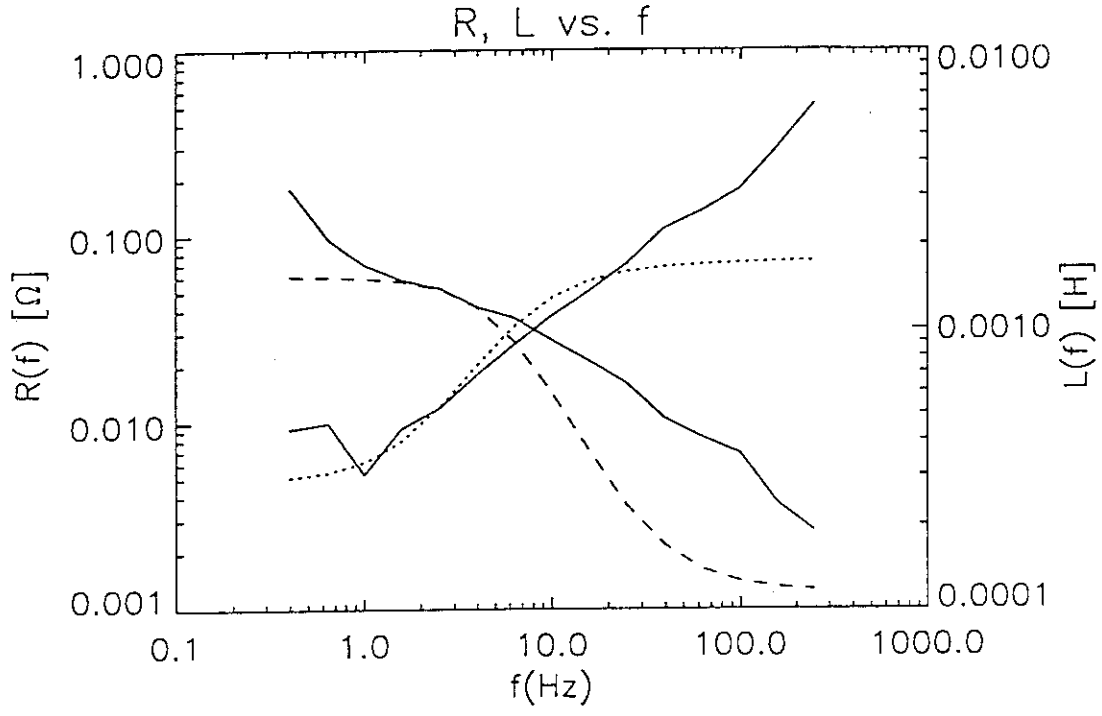

Fig. 8 Experimentally measured frequency response of H-coil and simulation with modified conductor model. Solid lines are experimental data, dashed and dotted are simulation data.

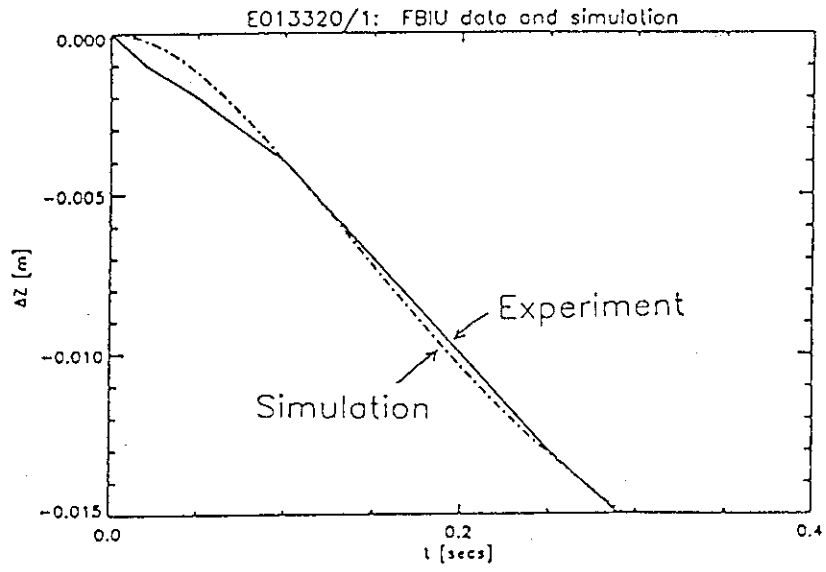

Fig. 9 Feedback turnoff experiment of 300 msec duration. (a) shows vertical position calculated from magnetic measurements, (b) compares experimental position data to simulation.

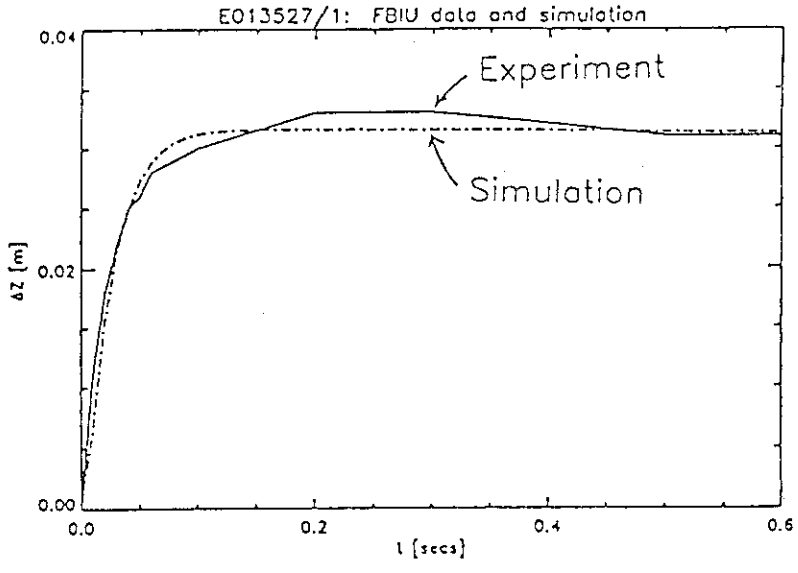

Fig. 10 Feedback turnoff experiment of 600 msec duration. (a) shows vertical position calculated from magnetic measurements, (b) compares experimental position data to simulation.

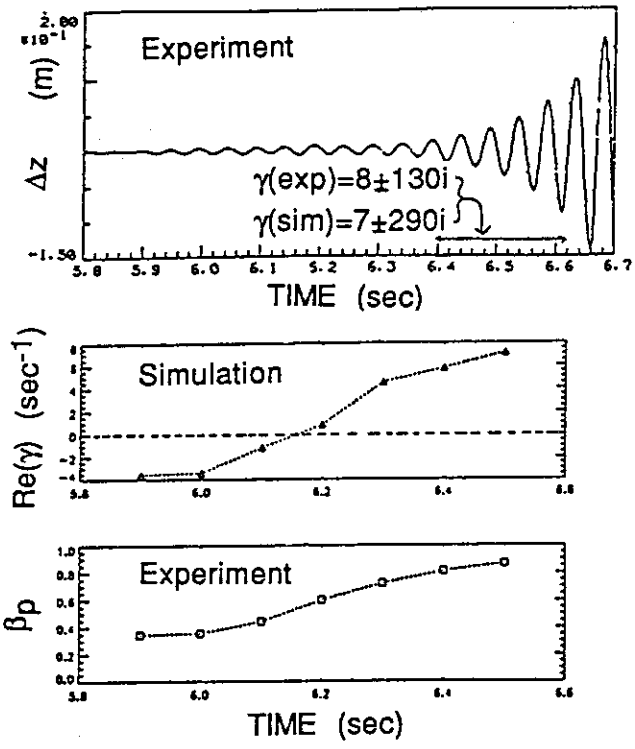

Fig. 11 NBI heated high β_p case 1: (a) vertical position, (b) simulation calculated growth rate, (c) β_p evolution.

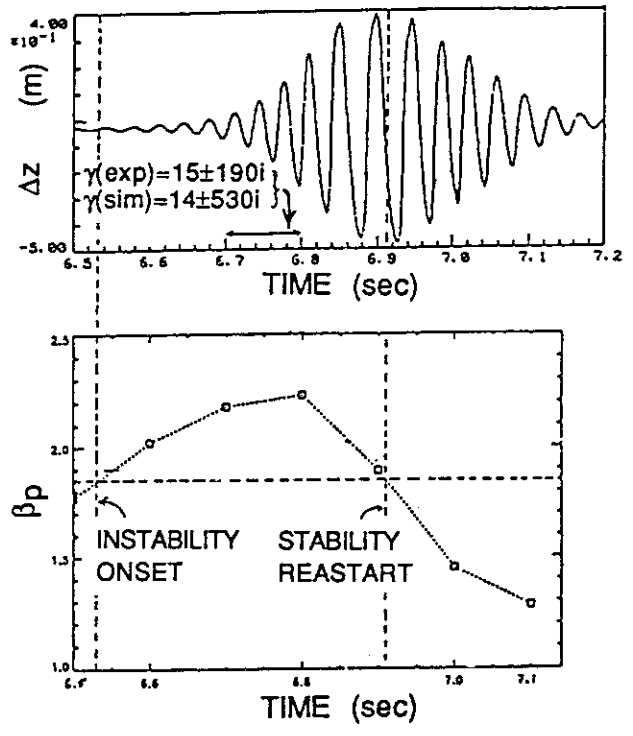

Fig. 12 NBI heated high β_p case 2: (a) vertical position, (b) β_p evolution.

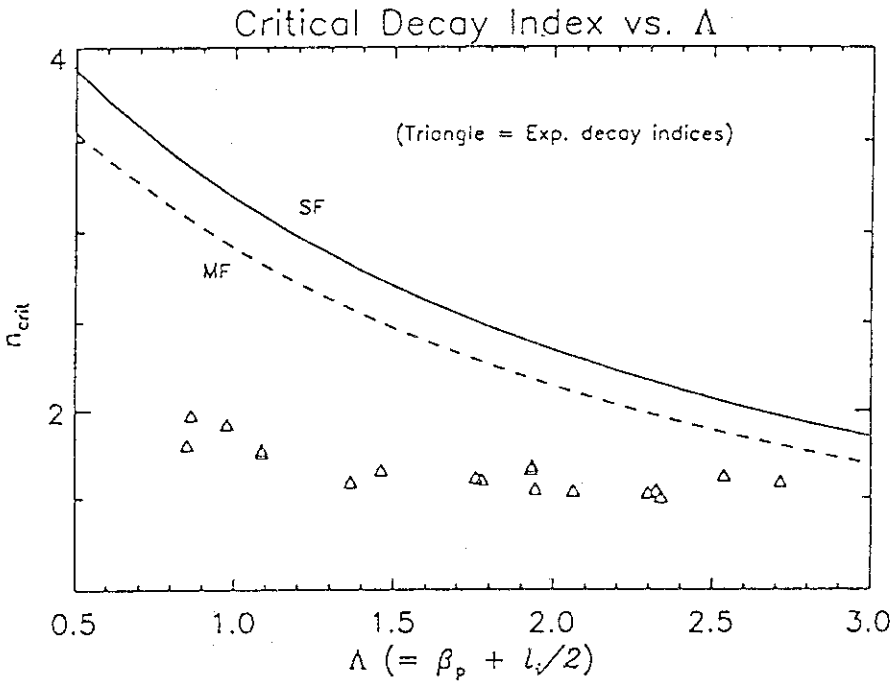

Fig. 13 Critical decay index and experimentally achieved decay indices vs. Shafranov Λ.

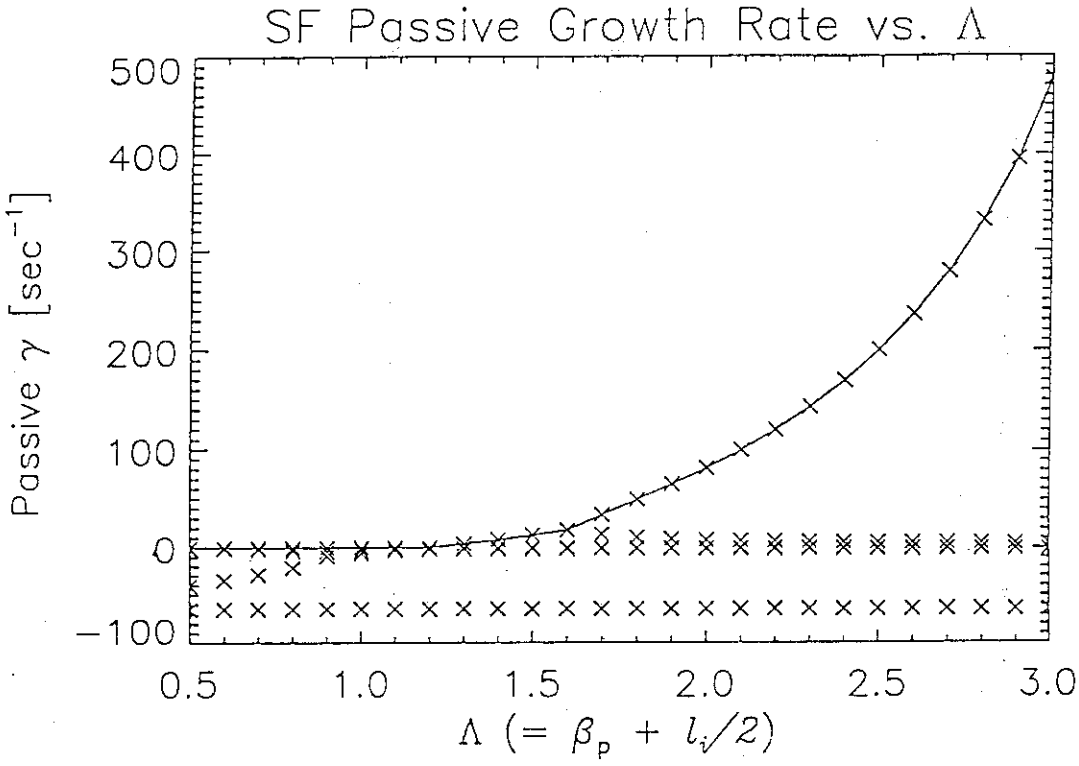

Fig. 14 Passive growth rates as a function of Λ for n=-1.6.

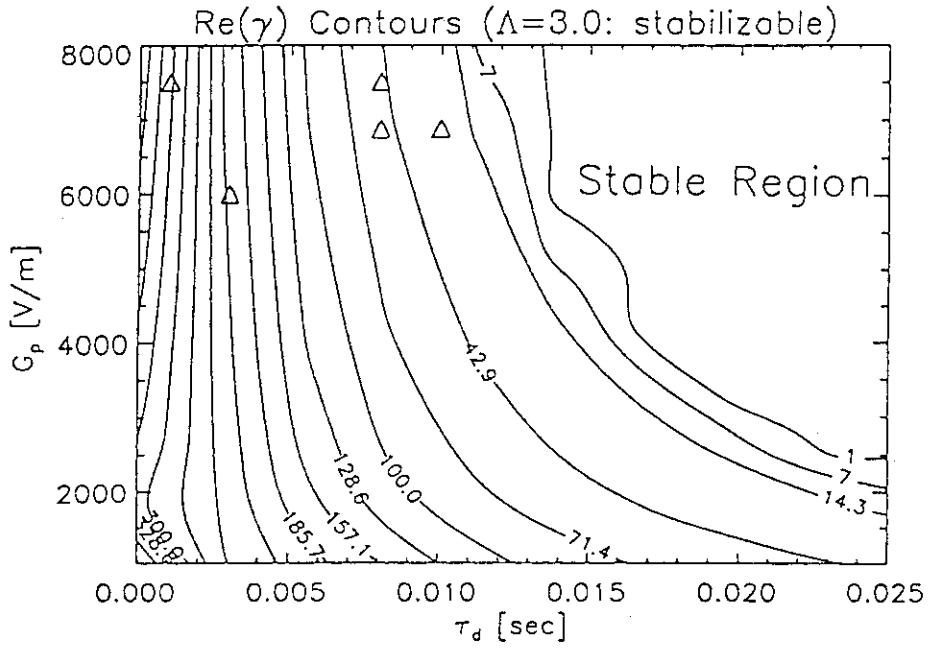

Fig. 15 Contours of constant growth rate in G_p and τ_d space showing stability boundary for Λ=3.0, n=-1.6. Triangles indicate typical operating points.

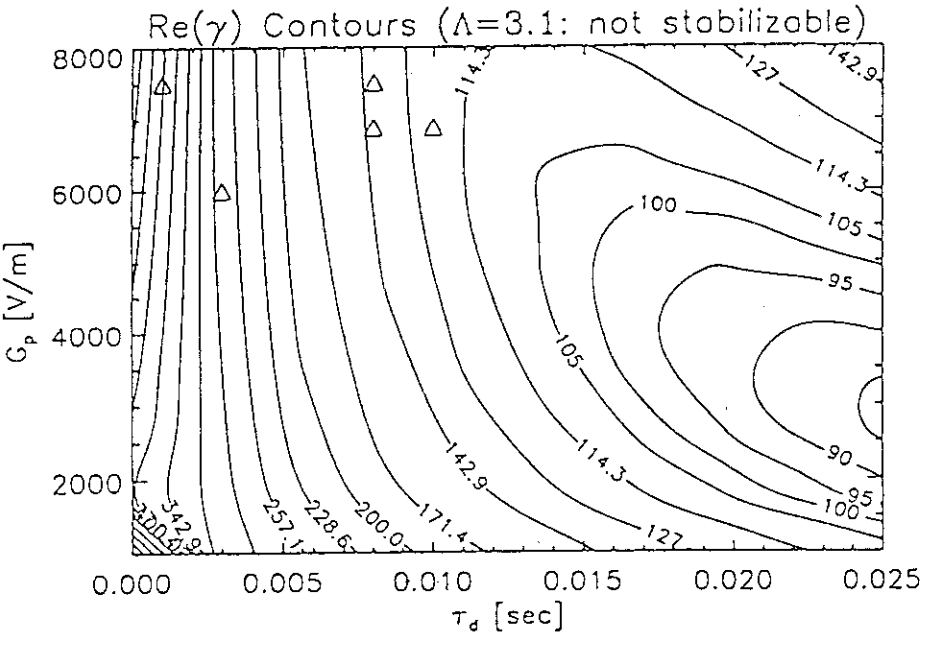

Fig. 16 Contours of constant growth rate in G_p and τ_d space showing no region of stability for Λ=3.1, n=-1.6. Triangles indicate typical operating points.